

pubs.acs.org/JPCB Article

Interfacial and Solution Aggregation Behavior of a Series of Bioinspired Rhamnolipid Congeners Rha-C14-Cx (x = 6, 8, 10, 12, 14)

Ricardo Palos Pacheco, Laurel L. Kegel, and Jeanne E. Pemberton*



Cite This: J. Phys. Chem. B 2021, 125, 13585-13596



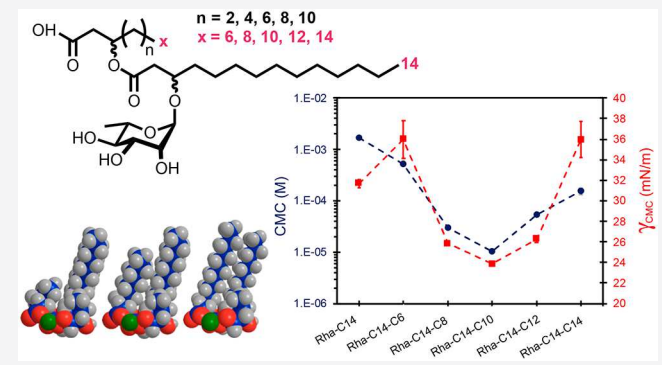
ACCESS

Metrics & More

Article Recommendations

3 Supporting Information

ABSTRACT: Rhamnolipids are glycolipids produced by microorganisms with outstanding surfactant properties. They are a class of biosurfactants that are potential candidates for biodegradable and nontoxic replacements of current specialty synthetic surfactants. Building on our previous efforts in developing an efficient and practical chemical methodology to synthesize rhamnolipids allows us to now explore the tunability of rhamnolipid properties. Here, we explore the impact on solution self-assembly and adsorption at the air/water interface of symmetry of the two lipid tails for diastereomeric mixtures of a series of monorhamnolipids of the generic structure Rha-C14-Cx. Surface activity of the anionic forms of these molecules at pH 8 is described by surface tensiometry. Characteristics of their



aggregation behavior in aqueous solutions including hydrodynamic radius, aggregation number, and aggregate morphology are determined using dynamic light scattering and time-resolved fluorescence quenching spectroscopy. The solution aggregation behavior of this series is found to unexpectedly vary in a nonmonotonic fashion. This is explained by molecular structural attributes of each series member that result in differences in the respective intermolecular interactions of various parts of these surfactants.

R hamnolipids are biosynthesized by several microorganisms $^{1-5}$ and have multiple biological roles. $^{6-13}$ Their structure is comprised of a lipid unit of (R,R)- β -hydroxyalkanoyl- β -hydroxyalkanoic acids¹⁴ of variable chain lengths $(C_6-C_{14})^{15,16}$ that are trans-1,2-O-glycosylated¹⁷ by monomeric or dimeric carbohydrate L-rhamnopyranosyl units. 18 These metabolites have attracted considerable attention due to their outstanding surfactant properties. 19,20 Rhamnolipids are one class of biosurfactants²¹ that have primarily found application in specialty surfactant sectors. 22-36 However, their incursion into wider markets has been hindered somewhat by the complexity of their structures, the difficulty of reliable and cost-effective methodologies that allow their manufacture at industrials scales, and the inability to tune their properties for specific applications. Successful technologies have been developed in this laboratory 19,37,38 that have enabled high-yield glycosylation of the aglycons of rhamnolipids with stable carbohydrate donors under benchtop conditions using mild and well-known solution-based transformations $^{39-42}$ and that allow manufacture of these materials at the kg scale. Nonetheless, even though our synthetic methods for rhamnolipids are efficient, flexible, scalable, green, and robust, they are not yet competitive with chemical procedures for manufacture of commercial counterparts such as sodium alkylsulfate, polyethoxylated surfactants, or the polyalkylglucosides that rely on building blocks based on petrochemicals.

Glycolipid surfactants can be manufactured from renewable feedstocks 43,44 and are becoming more attractive than petroleum-based surfactants due to their better biodegradability and lower toxicity. $^{45-47}$ With this interest in mind, it is important to understand the extent to which the properties of such materials can be intentionally designed with a precision that allows a priori fabrication of systems of controlled properties. Toward that end, we present here a structurefunction relationship study wherein monorhamnolipid properties are examined as a function of lipid tail symmetry. For this purpose, five bioinspired but not naturally occurring monorhamnolipid congeners obtained as diastereomeric mixtures of approximately equal amounts of (R,R), (R,S), (S,R), and (S,S) were synthesized containing a tetradecane (C14) lipid chain adjacent to the rhamnose sugar with a variable length carbon chain outer lipid tail to give the Rha-C14-C6, Rha-C14-C8, Rha-C14-C10, Rha-C14-C12, and Rha-C14-C14 congeners. We refer to this series as Rha-C14-Cx, and their members are shown in Figure 1. The concept of

Received: October 31, 2021
Revised: November 12, 2021
Published: December 3, 2021





Figure 1. Members of the Rha-C14-Cx series synthesized to evaluate the effect of the lipid tail symmetry on performance.

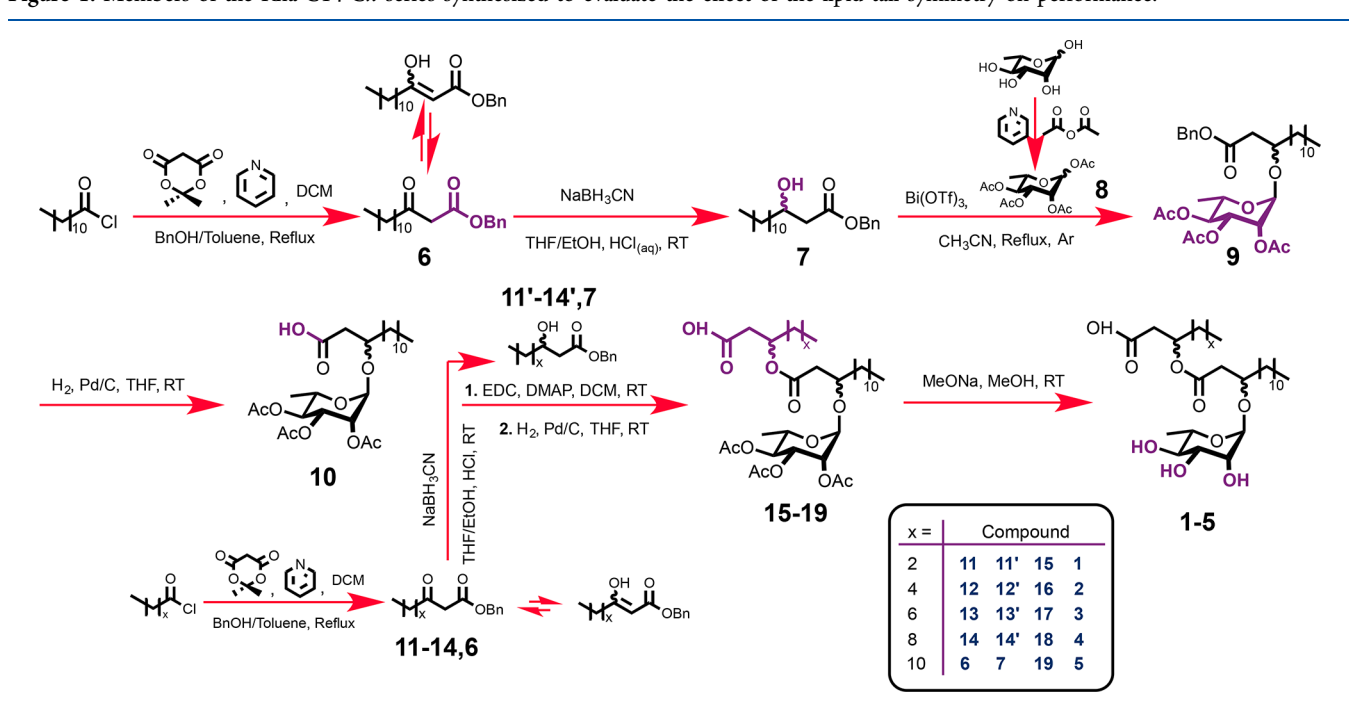


Figure 2. Synthetic methodology for manufacturing the members of the Rha-C14-Cx series.

bioinspiration is used here, since, although the range of individual lipid tail chain lengths used are found in nature, their combinations and absolute stereochemical configurations at the β -carbinols different than (R,R) are not available in nature.

The design of the five monorhamnolipid congeners as diastereomeric mixtures used here was based on the following considerations. First, from the thermodynamics of aggregation and interfacial adsorption of amphiphiles⁴⁸ and previous experiments on other monorhamnolipid congeners in our

laboratories, 19,38,49 we have learned that as the volume of the hydrophobic moiety is minimized, the surfactant performance gets poorer: single tail monorhamnolipids or double tail monorhamnolipids with shorter chains have higher critical aggregation concentrations (CAC) and lower affinity for the air—water interface (lower $K_{\rm ads}$). Second, the thermodynamic theory of self-assembly and the packing parameters derived therein $^{50-53}$ dictate that more conical surfactants will pack in more spherical aggregates whereas those that are more

cylindrical will pack in more lamellar structures. By creating a series of surfactants in which the inner chain length is maintained at 14 carbons while that of the outer chain is systematically varied from 6 to 14 carbons, we create a series of surfactants with molecular shapes ranging from conical to cylindrical whose packing properties were anticipated to systematically vary. Finally, our synthetic process results in diastereomeric mixtures of the congeners in which the attached β -hydroxyalkanoyl- β -hydroxyalkanoic acids are (R,R), (R,S), (S,R), or (S,S) in approximately equal amounts. ¹⁹ Indeed, our previous work showed that the aggregation behavior of such mixtures is similar to those of the individual diastereomers. although each individual diastereomer and the mixture are statistically distinguishable. 19,54–56 According to the thermodynamics of surfactant mixtures and the regular solution theory derived from it, 57-60 mixtures of stereochemically related surfactants with the same charge should have physicochemical solution and interfacial properties that are a calculable weighted average of the physicochemical solution and interfacial properties of the mixture components^{61,62} as proven in our laboratories for the diastereomers of Rha-C10-C10. 19

EXPERIMENTAL SECTION

Synthetic Methods. All members of the series are synthesized as diastereomeric mixtures following the methodology reported previously. 19,38 Generalities of the method are summarized here based on the scheme presented in Figure 2. Detailed synthetic procedures and supporting spectral characterization data are shown in the Supporting Information (Figures S1-S56, Tables S1 and S2). To synthesize these rhamnolipids, peracetylated anomeric mixtures of rhamnose are dissolved in refluxing acetonitrile (MeCN) in the presence of catalytic amounts of Bi(OTf)₃ to glycosylate a racemic mixture of a benzyl (\pm) -3-hydroxytetradecanoate ester. The glycosylation is stereoselective, and only the α -anomer is obtained due to the anomeric effect. The benzyl group of the resulting glycoside is cleaved by heterogeneous reductive hydrogenation in the presence of Pd/C in tetrahydrofuran (THF) at room temperature and pressure. The free acid is then esterified by using Steglich carbodiimide chemistry with the benzyl (rac)-3-hydroxyalkanoate ester of the proper hydrocarbon chain length (C6, C8, C10, C12, or C14). The resulting ester is debenzylated to render the free acid using the reductive hydrogenation noted above. The final products are obtained by a selective transesterification of the acetyl groups of the sugar unit under Zemplen conditions in the presence of MeONa/MeOH at room temperature. Each step of the synthetic methodology, except for the synthesis of the peracetylated rhamnose, requires isolation of the oily products by means of normal phase flash column chromatography. Characterization was performed by means of nuclear magnetic resonance (NMR) and mass spectrometry (MS). The purity of the final products was assessed by LC-MS.

Surface Tension Measurements. Surface tension measurements were performed at room temperature on a Fisher surface tensiometer model 21 by means of the Du Noüy ring method. Stock solutions of each of the Rha-C14-Cx series were prepared in Teflon vials equipped with Teflon-coated magnetic stir bars. The pH was adjusted to 8.0 by adding known minimum volumes of aqueous NaOH while stirring to make the respective anionic forms of the Rha-C14-Cx series. These stock solutions were stirred overnight at room temperature to guarantee complete dissolution of the

monorhamnolipids. Aliquots of the stock solutions of known volume were added to a known volume of water at pH 8.0 (adjusted with aqueous NaOH).

Dynamic Light Scattering. Dynamic light scattering (DLS) measurements were performed on a Viscotek 802 DLS⁶⁴ with a 50 mW fiber-coupled 830 nm diode laser. Hydrodynamic radii of aggregates in solutions of Rha-C14-Cx (x = 6, 8, 10, 12, 14) were characterized at concentrations from 1 to 35 mM. To prepare such solutions, the materials were dissolved in CH2Cl2 and transferred to 10 mL Teflon vials whereupon the solvent was removed under reduced pressure at 35 °C, and the masses were determined by difference to a constant weight. The remaining solids were dissolved in pH 8 aqueous 10 mM phosphate buffer and stirred overnight at room temperature after which the pH was readjusted to 8 with small amounts of aqueous NaOH if necessary and the solutions were equilibrated overnight again. Aliquots of the stock solutions were diluted with buffer to achieve 1 mL samples at concentrations of 1, 2.5, 5, 10, 15, 25, and 35 mM. Measurements were performed at 25 °C using 200 µL of solution dispensed from a 1000 μ L micropipette into a cuvette designed for DLS measurements that had been presilanized with tridecafluoro-1,1,2,2-tetrahydroctylsilane to prevent Rha-C14-Cx adsorption. DLS measurements consisted of 100 experiments with a duration of 5 s each over the period of 8 min. Regularization and regression analysis of the combined autocorrelation functions⁶⁵ was accomplished in Omnisize, the Viscotek analysis software, and yielded the mass distributions of aggregates at different concentrations.

Time-Resolved Fluorescence Quenching. Time-resolved fluorescence quenching (TRFQ) measurements were performed to assess aggregate polydispersity in 25 mM pH 8.0 solutions of the Rha-C14-Cx series. Stock solutions were prepared and stirred overnight. These were filtered with Acrodisc 25 mm syringe filters with 0.1 μ m Supor membranes (Pall Corporation). Pyrene was introduced by adding the appropriate amount of ~1 mM pyrene (Fluka, >99% pure, recrystallized) stock in cyclohexane (ACS grade, EMD) and allowing the cyclohexane to evaporate. The final pyrene concentration ([P]) was kept proportional to the Rha-C14-Cxmicelle concentration ([M]) at a ratio of [P]/[M] < 0.05 in order to maintain single occupancy at most and prevent excimer formation within micelles. 66,67 For solutions with benzophenone quencher (Q), the appropriate amount of \sim 75 mM benzophenone (Fluka, >99% pure, recrystallized) in cyclohexane or ethanol was added to the vial and allowed to evaporate at room temperature. The volume of the quencher aliquots used was chosen to produce values of η , the ratio of quenchers bound to aggregates, between 0.01 and 0.03. Solutions were thoroughly deoxygenated⁶⁸⁻⁷¹ by agitation in an environmental control chamber purged with Ar/N2 and stirred for at least 1 h for equilibration.

TRFQ measurements⁷² were performed at 25 °C under Ar using time-correlated single photon counting (TCSPC)⁷³ on a Quanta Master 40 spectrofluorometer (Photon Technologies, Inc.) Excitation was from a 340 nm LED (Photon Technologies, Inc.) with an excitation bandpass filter (340 \pm 10 nm, Edmund Optics). Emission was collected through an emission long-pass filter (364 nm, OD > 6, 300–363.8 nm, Semrock Inc.). Data were collected using Felix GX software version 4.1 for a range of 2000 ns, delay of 2200 ns, emission wavelength of 372 nm, offset of 15%, and binning of 1024 channels. Spectra were collected to an initial fluorescence

intensity of >10K counts. Slit widths were set such that the ADC signal was <2% of the LED pulse repetition rate, typically 1–1.5 mm. Measurements were made in capped, presilanized semimicro rectangular quartz cells (Starna Cells). Three replicate measurements each of three independently prepared solutions were averaged for each value of η .

Aggregation number is determined with TRFQ spectroscopy based on probe fluorescence decay by quenchers distributed within aggregates using a monoexponential fit based on the Tachiya–Infelta equation 74,75 to extract A_2 , A_3 , and A_4 parameters (see discussion in Supporting Information) with goodness of fit evaluated through multiple quantitative metrics (Durbin–Watson parameter, 76,77 ordinary runs test, reduced χ^2 , and correlation coefficient). Analysis of polydispersity is accomplished by plotting aggregation number at each quencher concentration $(N_{\text{agg},N})$ as a function of η . A weighted average aggregation number $(N_{\text{agg},N})$ and a number-average aggregation number $(N_{\text{agg},N})$ are calculated by fitting to the Grieser–Warr second and third order polynomials 78 with a standard deviation (σ) and skewness (λ) . Polydispersity is indicated when $N_{\text{agg},N} \not\approx N_{\text{agg},N}$.

indicated when $N_{\rm agg,w} \not\approx N_{\rm agg,N}$. Deviation of quenching kinetics due to the presence of aggregates larger than micelles was assessed by plotting $A_4/A_{\rm 4min}$ as a function of η (see Supporting Information). A_4 describes the rapid exponential decay at shorter times in the Tachiya–Infelta model and in the model proposed by Miller and Evans for vesicle-rich systems. Yariation in A_4 is due to partition of the quencher into aggregates with larger mass distributions first, with subsequent occupation of other aggregates with lower mass distributions as the quencher concentration increases. If the population of aggregates is multimodal with a wide range of geometries and sizes, the quenching kinetics will vary from population to population and be reflected in a convoluted fashion in the values calculated for A_4 using the Tachiya–Infelta equation.

Rha-C14-Cx Structure Energy Minimization. Three-dimensional structures of the Rha-C14-Cx series were energy minimized in Chem3D (version 19.1, PerkinElmer). The starting structure for these minimizations was taken to be that shown to have the value at which the minimum interfacial free energy per molecule is attained in our previous molecular dynamics (MD) simulations (i.e., 0.80 nm²). This molecular configuration was further energy minimized using both the MM2 and MMFF94 force fields to a gradient of 0.005 with similar results.

■ RESULTS AND DISCUSSION

Details of the synthetic work and structural characterization of the products and intermediates for the Rha-C14-Cx series are provided in the Supporting Information. Here, we describe the characterization of interfacial and self-assembly behavior of these molecules. Adsorption thermodynamics were determined by surface tension measurements, while solution assembly behavior was assessed using TRFQ and DLS.

Thermodynamics at the Air–Water Interface. Initial predictions about the air–water interface and solution assembly behavior of this rhamnolipid series come from consideration of the Tanford–Gruen–Israelachvili packing parameters (see Supporting Information for methods). 51,81,82 Proper estimation of hydrophobic tail dimensions requires accurate representation of molecular arrangement of the average monomer. This is not a trivial task for these molecules due to decentralization of the hydrophilic moieties in

rhamnolipids across the carboxylate, rhamnosyl unit, and the atoms at the 3-((3-hydroxypropanoyl)oxy)propanoic bridge that connect the two tails. From energy-minimized structures calculated in Chem3D using the MM2 force field (Figure 3;

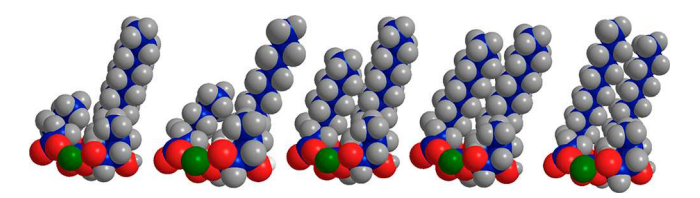


Figure 3. Space filling, energy-minimized pictures of the Rha-C14-C*x* series

similar structures obtained with the MMFF94 force field), the best representation of rhamnolipids involves a conformation in which the carboxylate is part of the hydrophilic headgroup, as represented in Figure 3. In this representation, the atoms of the 3-((3-hydroxypropanoyl)oxy)propanoic bridge are also part of the hydrophilic group resulting in a decrease in the effective number of methylene groups in each tail by three (see Figure S57). The area per molecule used for these packing parameter predictions, 0.80 nm², is that at which the minimum interfacial free energy per molecule is experienced from our previous molecular dynamics (MD) simulations of anionic rhamnolipids at the air-water interface.⁸⁰ With these constraints, the packing parameters estimated for this series ranges from 0.26 to 0.50 (Table S3). These values correspond to spherical micelles (P_c < 1/3) for Rha-C14 and Rha-C14-C6, ellipsoidal or cylindrical/rodlike micelles for Rha-C14-C8, Rha-C14-C10, and Rha-C14-C12, and vesicles/extended bilayers for Rha-C14-C14. 51,53,81,82 In fact, however, as recent MD simulations have demonstrated, 80,83 monorhamnolipids tend to pack in a variety of structures that range in size and with shape that vary from spherical to elongated, all with very similar energies. Given the propensity for this diversity in molecular conformation, and hence, molecular packing, these packing parameter predictions should be interpreted as guidelines for aggregates with the maximum order possible.

Adsorption characteristics of these rhamnolipids at the airwater interface were determined by surface tensiometry. Four parameters that describe this adsorption are considered here: critical micelle concentration (CMC), minimum surface tension ($\gamma_{\rm CMC}$), equilibrium adsorption constant ($K_{\rm ads}$), and surface area per molecule (a_0). Surface tension—concentration curves provide CMC and $\gamma_{\rm CMC}$ values directly. $K_{\rm ads}$ and a_0 values were determined by fitting the curves to the linear form (eq 2) of the Langmuir—Szyszkowski isotherm (eq 1), where n=2. Equations 2 and 3 were used to calculate a_0 , where N is Avogadro's number and ω is the area occupied per mole of surfactant.

$$\gamma = \gamma_0 - \frac{nRT}{\omega} \ln(1 + K_{\rm ad}C) \tag{1}$$

$$\gamma = \gamma_0 + \frac{n}{\omega} \Delta G_{\rm ad}^{\circ} - \frac{nRT}{\omega} \ln C \tag{2}$$

$$a_0 = \frac{\omega}{N \times 10^{-20}} \tag{3}$$

Figure 4a shows the surface tension—concentration behavior for the Rha-C14-Cx series along with the behavior for the single tail variant Rha-C14 for comparison. Figure 4b shows

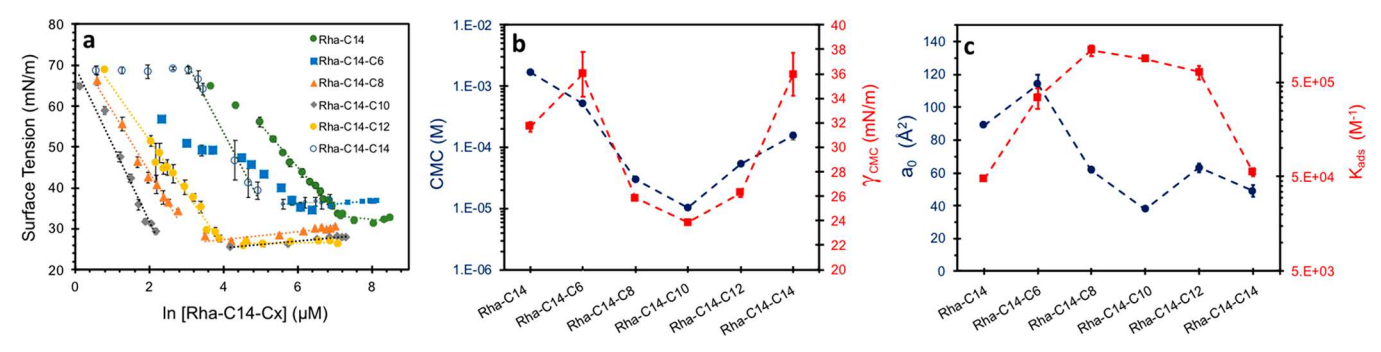


Figure 4. (a) Surface tension as a function of $\ln [Rha-C14-Cx]$, (b) critical micelle concentration (CMC) and minimum surface tension at the CMC (γ_{CMC}), and (c) adsorption equilibrium constant (K_{ads}) for adsorption at the air/water interface at pH 8.0 for Rha-C14-C6, Rha-C14-C8, Rha-C14-C10, Rha-C14-C12, and Rha-C14-C14. K_{ads} values were calculated from fitting to the linear form of the Langmuir–Szyszkowski equation.

values of critical micelle concentration (CMC) and minimum surface tension at the CMC ($\gamma_{\rm CMC}$) from fits to the Langmuir—Szyszkowski isotherm. Values for a_0 and $K_{\rm ads}$ from these fits are shown in Figure 4c. Numerical values for these parameters are provided in Table S4. In general, adding methylene groups to the second lipid tail reduces CMC and $\gamma_{\rm CMC}$ values; however, this does not occur in a monotonic fashion for the Rha-C14-Cx series. Surprisingly, for example, Rha-C14-C14 exhibits a $\gamma_{\rm CMC}$ value similar to those measured for Rha-C14-C6 and Rha-C14. Thus, the trends do not follow simple predictions based on hydrophobicity alone, i.e., reduction of CMC with hydrophobicity.

Comparing CMC and γ_{CMC} values for Rha-C14-C6 and Rha-C14-C8 reveals intriguing features about the inter- and intramolecular interactions that dictate structure-performance relationships. The structural difference between these two congeners is only two methylene groups, yet the effect on CMC and γ_{CMC} is large. The CMC for Rha-C14-C8 decreases by 95% and the γ_{CMC} value by 25% relative to the values measured for Rha-C14-C6. This is extraordinary given the structural similarities between these two congeners. Even more interesting, adding more methylene groups to the second tail to obtain surfactants with higher tail symmetry does not reduce the CMC and γ_{CMC} in a similar manner. Rha-C14-C10, Rha-C14-C12, and Rha-C14-C14 all have CMC values in the range of 10–150 μ M, with a slight local minimum for Rha-C14-C10 within this series. In contrast, CMC values for Rha-C14-C6 and Rha-C14 are in the mM regime, with a decrease of only ~70% in going from Rha-C14 to Rha-C14-C6 despite the addition of a 6-carbon chain in which at least two methylene groups and the methyl group reside in the hydrophobic portion of the tail. The change in γ_{CMC} values is even smaller, dropping only 4 mN/m when adding the second lipid tail. Also, it is intriguing that Rha-C14-C8, Rha-C14-C10, and Rha-C14-C12 have similar $\gamma_{\rm CMC}$ values, while Rha-C14-C14, the most hydrophobic of the series, resembles Rha-C14-C6 and Rha-C14. This unusual behavior was not predicted during molecular design of these materials wherein it was hypothesized that lipid tail symmetry would result in a more or less monotonic change in properties.

It is clear that the length of the outer lipid tail dictates surfactant performance in an unusual way. A general rule of thumb for surfactants is that the CMC should decrease by \sim 3-fold per additional methylene group. To rationalize the role of lipid tail symmetry in the Rha-C14-C α series, it is easiest to start by contrasting CMC values for Rha-C14-C6 and Rha-C14 whose CMCs differ by a factor of only 2 instead of by a factor

of ~9 as predicted by the general rule of thumb. Given that amphiphile aggregation is driven by the balance of opposing forces, 52,86,51,87 the length of the outer lipid tail of Rha-C14-C6 results in three conditions that work either independently or in combination to make air—water interface aggregation less spontaneous than expected: (i) the outer tail generates more steric hindrance in the hydrophobic core than the lipid tails of more symmetric members of the series, (ii) the relative absence of intramolecular interactions within the lipid tails influences the size of the hydrophilic headgroup, inducing greater headgroup—headgroup steric repulsions, and/or (iii) the outer lipid tail of Rha-C14-C6 is sufficiently short as to have essentially no or very weak hydrophobic interactions with surrounding lipid tails, thereby contributing little by way of hydrophobic stabilization to aggregation.

The trend in K_{ads} values as a funtion of lipid tail symmetry is also unforeseen in that affinity for the interface was expected to be directly proportional to size of the hydrophobic moiety. Instead, a downward parabolic dependence between K_{ads} and outer tail length is observed. Indeed, it is remarkable that Rha-C14 has an affinity for the interface similar to that of Rha-C14-C14, whereas both share a difference of more than an order of magnitude in $K_{\rm ads}$ compared with values for Rha-C14-C8, Rha-C14-C12, and Rha-C14-C10. It is noted that $K_{\rm ads}$ values align well with $\gamma_{\rm CMC}$ values, as $\gamma_{\rm CMC}$ is a parameter that clearly defines amphiphile effects on the assembly energetics at the air—water interface. Noteworthy is that the γ_{CMC} value for Rha-C14-C14 is close in value to those of the least hydrophobic congeners, Rha-C14 and Rha-C14-C6, revealing more about the nature of the intermolecular interactions at the interface of the highly hydrophobic and highly symmetric rhamnolipid surfactants.

Additional insight into the effects of asymmetric tails comes from analysis of the a_0 values shown in Figure 4c. Previous MD simulations of anionic Rha-C10-C10 at the air—water interface indicate an energetically preferred a_0 value of ~ 0.80 nm², a value that does not change much with surface concentration up to full monolayer coverage. That said, a_0 values ranging from 0.60 to 1.40 nm² were all found to be energetically accessible at room temperature in these simulations, differing in energy by $< 3 \text{ kcal/mol.}^{80}$ Significantly, at higher surface concentrations in these simulations with correspondingly smaller a_0 values, the monolayer begins to exhibit significant undulations, even resulting in near micelle formation at the interface.

The extent to which monolayers would exhibit such undulations is expected to be a function of the balance of possible headgroup—headgroup and tail—tail interactions. In

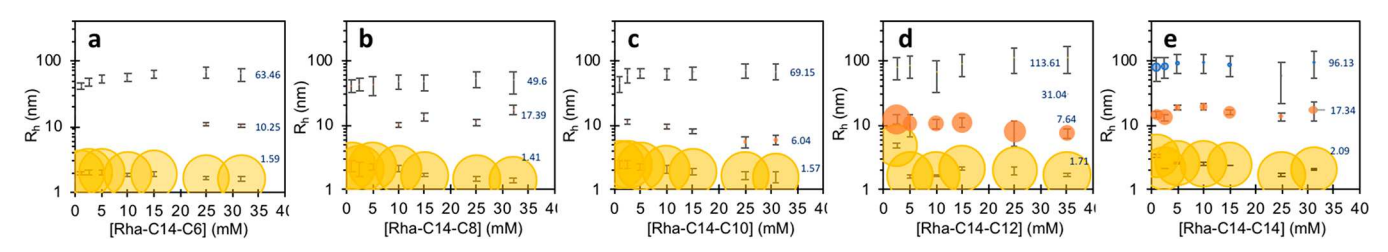


Figure 5. DLS mass distributions of hydrodynamic radii (R_h) of solution aggregates as a function of concentration at pH 8 for (a) Rha-C14-C6, (b) Rha-C14-C8, (c) Rha-C14-C10, (d) Rha-C14-C12, and (e) Rha-C14-C14. Bubble areas shown are proportional to the DLS peak area reported by the Viscotek analysis software, Omnisize. Error bars represent standard deviations of the peak hydrodynamic radii for a given aggregate size. Data points with only error bars visible represent aggregates with insignificant solution concentration.

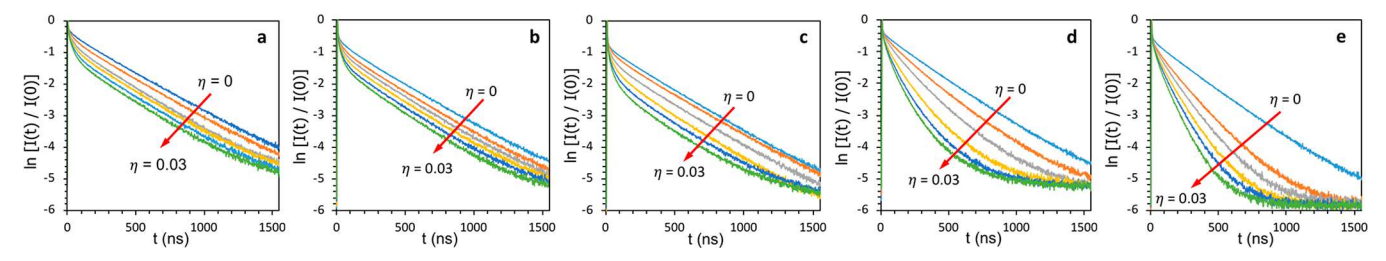


Figure 6. Time-resolved fluorescence decays for pyrene at 372 nm quenched with different concentrations (η) of benzophenone for 25 mM aqueous solutions at pH 8 for (a) Rha-C14-C6, (b) Rha-C14-C8, (c) Rha-C14-C10, (d) Rha-C14-C12, and (e) Rha-C14-C14.

this Rha-C14-Cx series, headgroup—headgroup interactions are expected to be constant whereas tail—tail interactions would be expected to increase with Cx chain length. Across this series, Rha-C14-C6 was found to have the largest a_0 value whereas those for Rha-C14-C8, Rha-C14-C10, Rha-C14-C12, and Rha-C14-C14 are smaller, consistent with this prediction. Although the possibility of differential adsorption of specific diastereomers must be considered, this is inconsistent with previous experimental work demonstrating only small differences between diastereomers. The observation of a large range of a_0 values despite changing only the hydrophobe suggests the dominance of both intra- and intermolecular hydrophobic interactions driving the formation of monolayer undulations.

The interplay of intramolecular hydrophobic interactions with headgroup conformation may also play a role in this behavior. In the absence of intramolecular hydrophobic interactions, as would be expected for Rha-C14-C6, the headgroup conformation may be more likely to attain what we have previously termed the fully open conformation on which the carboxylate group is the farthest from the rhamnose sugar. This conjecture aligns well with our explanation for larger CMC values for Rha-C14-C6 as well (vide supra). Hydrophobic intramolecular interactions between the lipid tails appear to increase for outer chains of C8 and longer. These forces may work to keep the two lipid tails closer in proximity, resulting in a partially closed or fully closed headgroup conformation on which the carboxylate group is closer to the rhamnose sugar leading to a consistently smaller value for a₀.

Self-Assembly in Solution: Dynamic Light Scattering. Figure 5 shows DLS mass distributions as a function of concentration for the Rha-C14-Cx series. Although these mass distributions provide only qualitative insight into the relative abundance of different aggregate populations, they are a useful indicator of microheterogeneity in complex surfactant environments. The corresponding number and intensity distributions are provided in Figure S58 in the Supporting Information. Two pieces of information are of interest: the hydrodynamic radii of

solution aggregates and the polydispersity as a function of concentration and lipid tail symmetry. In terms of polydispersity, the inventory of aggregate populations becomes more complex as lipid tail symmetry increases, although the hydrodynamic radii of the aggregates formed stays essentially constant as a function of concentration, with some appreciable changes in relative abundance. Larger aggregates are more readily seen in the intensity distributions (see Figure S58) due to their greater scattering cross sections. All Rha-C14-Cx solutions are rich in micellar aggregates of $R_{\rm h}$ = 1–2 nm with a relative abundance >90% for the concentrations studied. All surfactants also have at least two groups of larger aggregates whose relative abundances change slightly as a function of concentration: one group of $R_h = 5-20$ nm and a second of R_h = 50-100 nm that are likely unilamellar and mutilamellar vesicles. These larger aggregates are more abundant for Rha-C14-C12 and Rha-C14-C14. Concentration plays a minor role in aggregate size; however, as the tails become more symmetric, larger aggregates become more abundant due to the increased prominence of hydrophobic interactions that overcome headgroup-headgroup repulsive forces as the outer tail gets longer.

Time Resolved Fluorescence Quenching. Time resolved fluorescence quenching (TRFQ) experiments were performed to further assess aggregate polydispersity. For the ideal monodisperse micellar system, the fluorescence decay of pyrene quenched by benzophenone, with both components solubilized in surfactant aggregates, may be fit with the Tachiya–Infelta model (eq 4):

$$I(t) = I_0 e^{\{-A_2 t - A_3 (1 - e^{(-A_4 t)})\}}$$
(4)

where I_0 is the fluorescence intensity at time zero, I(t) is the fluorescence intensity at time t, and A_2 , A_3 , and A_4 are fitting parameters related to physical quantities as $A_2 = k_{\rm F} + [{\rm Q}](k_{\rm Q}/A_4)(k_{\rm A})(k_{\rm A})$, $A_3 = ([{\rm Q}]/[{\rm M}])(k_{\rm Q}/A_4)^2$, and $A_4 = k_{\rm Q} + k_{\rm A}$ in accordance with a system composed of a hydrophobic, immobile probe (here, pyrene), and a hydrophobic, potentially mobile quencher (here, benzophenone.) Here, $k_{\rm F}$ is the

radiative fluorescence rate constant, [Q] is the quencher concentration, k_Q is the quenching rate constant, k_{-} is the rate constant for quencher exit of an aggregate, and [M] is the micelle concentration. The qualitative features of these emission decays will be described here with detailed statistical analysis reserved for the Supporting Information.

Figure 6 shows semilogarithmic plots of the emission decays of pyrene fluorescence quenched by different concentrations of benzophenone in 25 mM aqueous solutions of the Rha-C14-Cx series at pH 8.0. Here, quencher concentration is expressed in terms of the parameter η , which represents the ratio of quenchers solubilized in aggregates defined by the approximation provided by eq 5:

$$\eta \approx \frac{\left[Q\right]_{\text{total}}}{\left[S\right]_{\text{total}} - \text{CMC}}$$
(5)

where $[Q]_{total}$ is the total concentration of quencher added and $([S]_{total} - CMC)$ is the concentration of total surfactant that exists in aggregates.

The quenching profiles in Figure 6 demonstrate that lipid tail symmetry has a profound effect on the fluorescence quenching of solubilized pyrene. The model parameters in eq 4 were computed by nonlinear least-squares based on the Marquardt algorithm.⁹¹ The goodness of fit to this model can be evaluated by visual inspection of the residuals (Figure S59) and through the use of several quantitative statistical parameters and methods: reduced χ^2 , Durbin-Watson (DW) test, and runs test (see Figure S60). Visual inspection of the residuals (Figure S59) reveals greater bias in fitting for the decays from Rha-C14-C10, Rha-C14-C12, and Rha-C14-C14. These residuals exhibit a structured, nonrandom deviation within the first 200 ns that becomes more pronounced for these members of the series. The quantitative metrics displayed in Figure S60 further confirm these deviations for the longer chain members of the series. Defining a good fit as $\chi^2 < 1.7$, DW > 1.6, and runs test = 0, the results in Figure S60 confirm that only fits to the decays for Rha-C14-C6 and Rha-C14-C8 at any value of η fulfill these criteria. Poorer fits are observed for the Rha-C14-C10, Rha-C14-C12, and Rha-C14-C14 in agreement with inspection of the residuals. The micellar Tachiya-Infelta equation models the data well for Rha-C14-C6 and Rha-C14-C8, indicating micellar systems together with other information herein, and poorly for the Rha-C14-C10, Rha-C14-C12, and Rha-C14-C14 series, indicating polydisperse aggregates and/or mobility of pyrene/benzophenone.

Fluorescence decay profiles provide qualitative insight into the morphology and dynamics of these aggregates. For example, micelle-rich systems with no quencher migration show fluorescence decays with (1) a fast multiexponential decay at very short times from probes quenched within micelle compartments, and (2) exponential emission decay at longer times from unquenched fluorescence decay (i.e., linear on semilogarithmic plot) that parallels the decay without quencher (i.e., at $\eta = 0$.) Specifically, these characteristics are exhibited by the decay profiles from Rha-C14-C6 and Rha-C14-C8. In contrast, the decay profiles for quenching in the microheterogeneous solutions of Rha-C14-C10, Rha-C14-C12, and Rha-C14-C14 lack the initial fast decay; instead, the initial decay looks almost exponential followed by a long, weak curvature. At higher values of η and long times, the emission decays from Rha-C14-C12 and Rha-C14-C14 (and for Rha-C14-C10 to a lesser extent) are not parallel with those at $\eta = 0$.

This behavior may be attributable to relocation of the quencher to bulk water or a change in the microenvironment of the quencher during the experimental window. However, for Rha-C14-C10, Rha-C14-C12, and Rha-C14-C14, the emission decay profile likely changes with quencher concentration because of quencher partitioning into aggregates of different sizes, consistent with a polydisperse aggregate population as indicated by DLS.

On the basis of previous detailed numerical analysis⁷⁹ and TRFQ results of microheterogeneous solutions, ^{92–94} the emission decays for pyrene in solutions of Rha-C14-C10, Rha-C14-C12, and Rha-C14-C14 are indicative of an aggregate mixture of different morphologies, with aggregates of large size dominating quencher partitioning due to their large mass fraction. Emission quenching in these kinds of mixtures is not adequately described by the Tachiya–Infelta model. ^{95,96} Instead, eq 6 describes the emission decay for quenching in solutions containing only large volume vesicles:

$$I(t) = I_0 e^{\{-A_5 t - A_6 t^{1/2}\}}$$
(6)

where A_5 is related to Stern–Volmer kinetics and A_6 is related to diffusion depletion. ^{97,98} In theory, the weighted sum of eqs 4 and 6 should describe the emission quenching in a microheterogeneous solution containing a mixture of micelles and vesicles. ⁷⁹ Unfortunately, this model requires fitting to eight variables, which is intractable.

The Tachiya—Infelta model is the best studied and most tested model used to describe TRFQ in microheterogeneous solutions, and it has been shown through data simulation that ill-fitted data can still be used for qualitative comparative diagnostics about aggregation behavior. Therefore, absent a rigorous quantitative solution for the Rha-C14-C10, Rha-C14-C12, and Rha-C14-C14 decays due to polydispersity, the fits from the Tachiya—Infelta model are used here as qualitative indicators of aggregation such that comparisons with the data from Rha-C14-C6 and Rha-C14-C8, which are well-fit by the model, can be made. Detailed analysis of parameters from fits to the Tachiya—Infelta model are considered in the Supporting Information. The following two sections consider additional insight from these fits about aggregate polydispersity, quencher migration, and vesicle concentration.

Aggregate Polydispersity. One of the main purposes of these experiments was to evaluate aggregation number, $N_{\rm agg}$, polydispersity from the parameters A_2 and A_3 of the Tachiya—Infelta model (eq 4). §8,99,100 If $N_{\rm agg}$ is constant with η for constant surfactant and probe concentration, the system is considered to be monodisperse. Conversely, if $N_{\rm agg}$ changes as a function of quencher concentration (expressed as η for $0 \le \eta \le 0.03$), then the aggregates are polydisperse. This dependence on η arises from the progressive partitioning of quencher into the increasingly less mass abundant, less hydrophobic aggregates. $N_{\rm agg,\eta}$ is used in Figure 7 to represent the apparent aggregation values as a function of η . Details of the second and third order fits to these plots are given in Table S5. The relevant fitting parameters for calculating a weighted average aggregation number $N_{\rm agg,w}$ according to the Grieser-Warr equation $N_{\rm agg}$ are given in Table 1. The profiles of these fits provide information about aggregate polydispersity.

Figure 7 shows that $N_{\text{agg},\eta}$ is largely independent of η for aggregates of Rha-C14-C6 indicating that they are monodisperse. The small slopes of the second and third order fits in Table S4 for Rha-C14-C6 support a narrow size distribution.

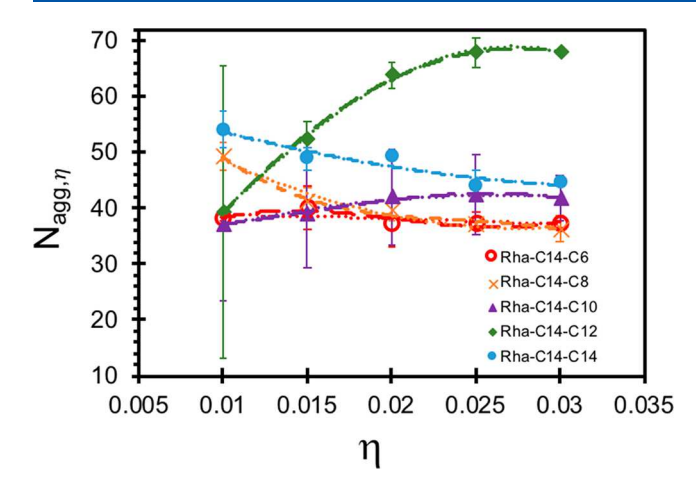


Figure 7. $N_{\text{agg}\eta\eta} - \eta$ curves of the members of the Rha-C14-Cx series fit to second and third order polynomials of the Grieser–Warr equation.

In contrast, aggregates of Rha-C14-C8 are more polydisperse, as indicated by both the $N_{\rm agg,\eta}-\eta$ plots as well as the polynomial fits. This polydispersity is likely due, at least in part, to the presence of a small population of vesicles, consistent with the DLS results. The polydispersity for Rha-C14-C10, Rha-C14-C12, and Rha-C14-C14 cannot be accurately extracted from these results due to the poor fit to the Tachiya–Infelta model. Although the data for Rha-C14-C10, Rha-C14-C12, and Rha-C14-C14 are clearly indicative of polydispersity, further quantitative inferences cannot be made.

The Supporting Information contains additional evidence for aggregate polydispersity with discussion from a detailed analysis of the TRFQ decays for determination of A_2 , k_- , A_4 , and $A_4/A_{4\text{min}}$. These results are shown in Figure S61 and S62 and Table S6 and support the conclusions above of polydisperse solutions for Rha-C14-C10, Rha-C14-C12, and Rha-C14-C14 but not Rh-C14-C6 or Rha-C14-C8.

Aggregate Microenvironment. The pyrene emission lifetime also reports on the average polarity of its microenvironment, 66,101,102 thereby allowing comparisons with other surfactant systems. In principle, as the local hydrophobicity increases (i.e., polarity decreases), the excited state lifetime, τ , estimated as the slope of a straight line fit to a semilogarithmic decay, increases, because excited states are typically more polar than the corresponding ground states and vibronically couple less well with a surrounding nonpolar solvent. For example, the pyrene lifetime is known to be considerably longer in cyclohexane (408 \pm 5 ns) than in water (226 \pm 10 ns). 101

The environment seen by a probe in a microheterogeneous solution is dictated by aggregate morphology, probe polarity, amphiphile molecular structure, distance of the probe from the amphiphile headgroup, temperature, amphiphile packings, viscosity, and the penetration of water into aggregates. Due to this large number of factors that influence local environment, it is impossible to develop a comprehensive description of possible probe microenvironments for a given aggregate. Nonetheless, insights and relative generalizations can be made.

Figure 8 shows the semilogarithmic emission decays (inset) for pyrene in Rha-C14-Cx aggregates and the corresponding

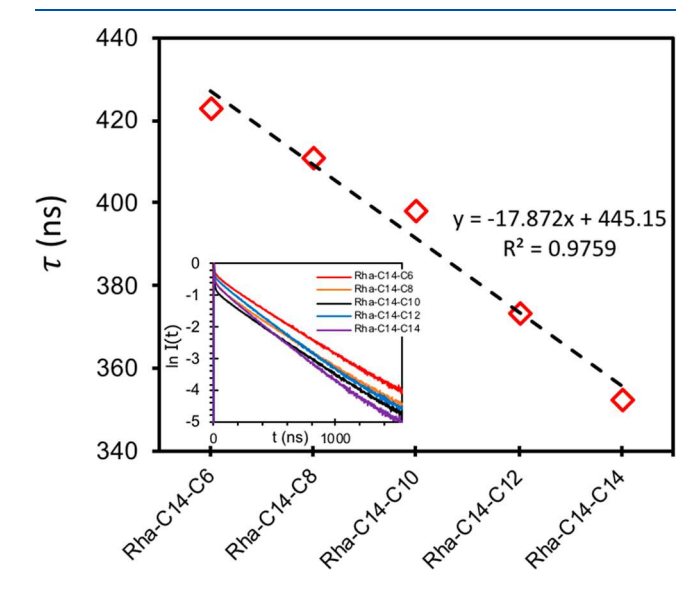


Figure 8. Pyrene lifetimes from fitting semilogarithmic fluorescence emission decays (inset) to eq 4 for the Rha-C14-C*x* series.

lifetimes from these decays. In principle, the longer is the lifetime, the lower is the polarity of the microenvironment surrounding the fluorescent probe. Interestingly, the lifetime for Rha-C14-C6 and Rha-C14-C8 is higher than that observed in cyclohexane, and a decrease in pyrene lifetime is observed as the lipid tails become more symmetric. At first glance, this observation is counterintuitive, since one would expect more hydrophobic microenvironments for pyrene as the chains become more symmetric. Why the observed microenvironment follows the opposite behavior becomes even more intriguing when considering that polyaromatic probes generally experience greater polarity in aggregates of greater surface

Table 1. Polydispersity Parameters of the Aggregation Number for Second and Third Order Polynomial Fits

surfactant	polynomial order	$N_{ m agg,w}$	σ^a	λ^{b}	$oldsymbol{arepsilon}^c$	R^2	polydispersity
Rha-C14-C6	2	39	6	-40		0.3011	no ^d
	3	17	87	-0.9	-0.5	0.7119	yes ^d
Rha-C14-C8	2	67	66	0.4		0.963	yes
	3	88	110	0.6	-0.31	0.9882	yes
Rha-C14-C10	2	28	46	-0.6		0.9583	yes
	3	36	26	9	5.86	0.9758	yes
Rha-C14-C12	2	4	10	-0.3		0.9976	yes
	3	5	87	-0.05	-0.32	0.9983	yes
Rha-C14-C14	2	63	46	0.5		0.8866	yes
	3	62	45	0.4	-0.42	0.8866	yes

 $^{{}^{}a}\sigma$ = standard deviation for a Gaussian distribution. ${}^{b}\lambda$ = skewness standardized to a Gaussian distribution. ${}^{c}\varepsilon$ = kurtosis standardized to a Gaussian distribution. ${}^{d}F$ itting to either second or third order polynomial results in poor fit.

curvature due to the penetration of water. Yet, for Rha-C14-Cx, in the surfactant solution richest in micelles, Rha-C14-C6, the longest lifetime is observed.

Detailed descriptions of pyrene photophysics indicate that pyrene tends to reside close to the polar headgroups of surfactant aggregates 89,102 due to polar headgroup— π interactions. It is further known that such interactions with the sugar occur in an additive and cooperative fashion for aromatic probes such as pyrene as a consequence of inductive electronic effects provided by the sugar heteroatoms that enhance these interactions. This unexpected behavior in microenvironment polarity across the Rha-C14-Cx series can be rationalized by considering the effects of aggregate core free volume and the consequent ability of aggregates to incorporate pyrene in this region.

The detailed analysis of the surface tensiometry results described above supports the assertion that highly asymmetric congeners such as Rha-C14-C6 have relatively weak or nonexistent interlipid interactions due to the large size of the headgroup, making the lipid tails more flexible and, in the presence of a constant headgroup volume across the series, with more free volume to incorporate pyrene within the core. In contrast, as lipid tail symmetry increases, both intra- and intermolecular interactions between the chains increase substantially and free volume within the core that could accommodate pyrene rapidly decreases, thereby forcing the pyrene to reside closer to the more congested polar headgroup region. This picture for symmetric lipid tail packing is wholly consistent with the results of molecular dynamics simulations reported previously from these laboratories which show that despite somewhat disordered lipid tails, the aggregate cores exhibit a distinct lack of free volume to accommodate additional molecules. 80,83,110 These simulations further indicate significant disruption of monorhamnolipid packing in aggregates upon incorporation of even small numbers of nonpolar molecules in their cores, ¹¹⁰ making this incorporation energetically unfavorable as concluded here. In summary, the fluorescence lifetime studies support a picture in which pyrene exists in the more nonpolar core of the less symmetric members of Rha-C14-Cx but which is progressively pushed outward toward the more polar headgroups of the aggregates as chain symmetry increases to Rha-C14-C14.

CONCLUSIONS

The overall purpose of the work reported here was to assess whether and to what extent the surfactant properties of rhamnolipids could be tuned by design. The original intent of the molecular design was to tune properties more or less monotonically based on overall molecular shape. This vision assumed a constant headgroup volume, requiring a constant headgroup conformation. However, somewhat unexpectedly, the interfacial properties of these materials were found to be largely controlled by the structure and hydrophobic properties of the lipid tails that drive changes in headgroup conformation and hence headgroup volume, which is wholly consistent with previous molecular dynamics simulations on structurally related rhamnolipid systems. These changes also strongly impact the solution aggregation behavior as expected based on packing predictions with larger and more complex aggregates forming as lipid tail symmetry increases. Rha-C14-C6 and Rha-C14-C8 form largely micellar solutions with aggregation numbers of 39 and 67, respectively. In contrast, Rha-C14-C10, Rha-C14-C12, and Rha-C14-C14 generally form larger

aggregates such as vesicles or multilamellar structures with aggregation numbers that could not be accurately defined using the methods employed here. Interestingly, little change is observed in the inventory with changes in concentration over the range of surfactant concentrations explored (0.1–30 mM).

The average microenvironment experienced by a pyrene fluorescent probe within the aggregates is affected by the lipid tail symmetry with average polarity of the aggregates increasing as the lipid tails become more symmetric. This behavior is contrary to that previously reported for other surfactant systems in which larger aggregates have less polar core microenvironments. This apparent contradiction is rationalized in terms of the interlipid interaction strength and its effect on core free volume. Strong interlipid interactions of symmetric lipid tails drive changes in headgroup conformation and push the pyrene probe outward toward the more polar headgroup region.

Overall, changes in lipid tail symmetry and molecular packing due to aggregate shape across the Rha-C14-Cx series have a powerful impact on both the interfacial properties and the self-assembly behavior but not in a systematically varying manner. This work provides considerable insight into the complexities of the rhamnolipid molecular structural attributes that contribute to self-assembly and the ability to sequester other molecules. We expect that these results will be valuable for other researchers attempting to design synthetic rhamnolipids for specific applications.

ASSOCIATED CONTENT

Supporting Information

The Supporting Information is available free of charge at https://pubs.acs.org/doi/10.1021/acs.jpcb.1c09435.

Detailed descriptions of synthetic methods for the Rha-C14-Cx series, all supporting spectroscopic characterization data, additional information on packing parameter predictions, the surface tension and dynamic light scattering measurements, and detailed analyses of the TRFQ decay profiles based on the Tachiya–Infelta model (PDF)

Special Issue Paper

This paper was intended for the 125 Years of *The Journal of Physical Chemistry* Virtual Special Issue, published December 2, 2021.

AUTHOR INFORMATION

Corresponding Author

Jeanne E. Pemberton — Department of Chemistry and Biochemistry, University of Arizona, Tucson, Arizona 85721, United States; orcid.org/0000-0002-1710-2922; Email: pembertn@email.arizona.edu

Authors

Ricardo Palos Pacheco — Department of Chemistry and Biochemistry, University of Arizona, Tucson, Arizona 85721, United States; Present Address: Bio-Rad Laboratories, Inc., 5731 W Las Positas Boulevard, Pleasanton, CA 94588, United States

Laurel L. Kegel – Department of Chemistry and Biochemistry, University of Arizona, Tucson, Arizona 85721, United States; Present Address: Bachem Americas, Inc., 3132 Kashiwa Street, Torrance, CA 90505, United States

Complete contact information is available at:

https://pubs.acs.org/10.1021/acs.jpcb.1c09435

Author Contributions

All authors have given approval to the final version of the manuscript.

Notes

The authors declare the following competing financial interest(s): J.E.P. has equity ownership in GlycoSurf, Inc. that is developing products related to the research being reported. The terms of this arrangement have been reviewed and approved by the University of Arizona in accordance with its policy on objectivity in research.

ACKNOWLEDGMENTS

The authors gratefully acknowledge support of this research through funding from the National Science Foundation (Grants CHE-1339597 and CHE-1954467). R.P.P. gratefully acknowledges the additional fellowship support from Consejo Nacional de Ciencia y Tecnología (CONACyT) and Secretaría de Educación Pública (SEP) of México to complete his doctoral studies. The authors acknowledge valuable discussions with Professor Robin Polt about some of the synthetic aspects of this work.

REFERENCES

- (1) Soberón-Chávez, G.; Lépine, F.; Déziel, E. Production of rhamnolipids by *Pseudomonas aeruginosa*. *Appl. Microbiol. Biotechnol.* **2005**, *68*, 718–725.
- (2) Hori, K.; Ichinohe, R.; Unno, H.; Marsudi, S. Simultaneous Syntheses of Polyhydroxyalkanoates and rhamnolipids by *Pseudomonas aeruginosa* IFO 3924 at various temperatures and from various fatty acids. *Biochem. Eng. J.* 2011, 53, 196–202.
- (3) Hörmann, B.; Müller, M. M.; Syldatk, C.; Hausmann, R. Rhamnolipid production by *Burkholderia plantarii* DSM 9509T. *Eur. J. Lipid Sci. Technol.* **2010**, *112*, 674–680.
- (4) Clarke, K. G.; Ballot, F.; Reid, S. J. Enhanced Rhamnolipid Production by *Pseudomonas aeruginosa* under Phosphate Limitation. *World J. Microbiol. Biotechnol.* **2010**, 26, 2179–2184.
- (5) Abdel-Mawgoud, A. M.; Lépine, F.; Déziel, E. Rhamnolipids: Diversity of Structures, Microbial Origins and Roles. *Appl. Microbiol. Biotechnol.* **2010**, *86*, 1323–1336.
- (6) Solano, C.; Echeverz, M.; Lasa, I. Biofilm Dispersion and Quorum Sensing. *Curr. Opin. Microbiol.* **2014**, *18*, 96–104.
- (7) Nickzad, A.; Déziel, E. The Involvement of Rhamnolipids in Microbial Cell Adhesion and Biofilm Development An Approach for Control? *Lett. Appl. Microbiol.* **2014**, *58*, 447–453.
- (8) Abalos, A.; Pinazo, A.; Infante, M. R.; Casals, M.; García, F.; Manresa, A. Physicochemical and Antimicrobial Properties of New Rhamnolipids Produced by *Pseudomonas aeruginosa* AT10 from Soybean Oil Refinery Wastes. *Langmuir* **2001**, *17*, 1367–1371.
- (9) Arino, S.; Marchal, R.; Vandecasteele, J.-P. Involvement of a Rhamnolipid-Producing Strain of *Pseudomonas aeruginosa* in the Degradation of Polycyclic Aromatic Hydrocarbons by a Bacterial Community. *J. Appl. Microbiol.* **1998**, *84*, 769–776.
- (10) Itoh, S.; Suzuki, T. Effect of Rhamnolipids on Growth of *Pseudomonas aeruginosa* Mutant Deficient in n-Paraffin-utilizing Ability. *Agric. Biol. Chem.* **1972**, *36*, 2233–2235.
- (11) Andra, J.; Rademann, J.; Howe, J.; Koch, M. H. J.; Heine, H.; Zahringer, U.; Brandenburg, K. Endotoxin-like Properties of a Rhamnolipid Exotoxin from *Burkholderia (Pseudomonas) plantarii*: Immune Cell Stimulation and Biophysical Characterization. *Biol. Chem.* **2006**, 387, 301–310.
- (12) Tremblay, J.; Richardson, A. P.; Lépine, F.; Déziel, E. Self-Produced Extracellular Stimuli Modulate the *Pseudomonas aeruginosa* Swarming Motility Behavior. *Environ. Microbiol.* **2007**, *9*, 2622–2630.

- (13) Murray, T. S.; Kazmierczak, B. I. *Pseudomonas aeruginosa* Exhibits Sliding Motility in the Absence of Type IV Pili and Flagella. *J. Bacteriol.* **2008**, *190*, 2700–2708.
- (14) Nakagawa, Y.; Matsuyama, T. Chromatographic Determination of Optical Configuration of 3-Hydroxy Fatty Acids Composing Microbial Surfactants. FEMS Microbiol. Lett. 1993, 108, 99–102.
- (15) Benincasa, M.; Abalos, A.; Oliveira, I.; Manresa, A. Chemical Structure, Surface Properties and Biological Activities of the Biosurfactant Produced by *Pseudomonas aeruginosa* LBI from Soapstock. *Antonie van Leeuwenhoek* **2004**, *85*, 1–8.
- (16) Haba, E.; Pinazo, A.; Pons, R.; Pérez, L.; Manresa, A. Complex Rhamnolipid Mixture Characterization and Its Influence on DPPC Bilayer Organization. *Biochim. Biophys. Acta, Biomembr.* **2014**, *1838*, 776–783.
- (17) Edwards, J. R.; Hayashi, J. A. Structure of a Rhamnolipid from *Pseudomonas aeruginosa*. Arch. Biochem. Biophys. **1965**, 111, 415–421.
- (18) Jarvis, F. G.; Johnson, M. J. A Glycolipid Produced by Pseudomonas aeruginosa. J. Am. Chem. Soc. 1949, 71, 4124-4126.
- (19) Palos Pacheco, R.; Eismin, R. J.; Coss, C. S.; Wang, H.; Maier, R. M.; Polt, R.; Pemberton, J. E. Synthesis and Characterization of Four Diastereomers of Monorhamnolipids. *J. Am. Chem. Soc.* **2017**, 139, 5125–5132.
- (20) Kutschmann, E. M.; Findenegg, G. H.; Nickel, D.; von Rybinski, W. Interfacial Tension of Alkylglucosides in Different APG/Oil/Water Systems. *Colloid Polym. Sci.* 1995, 273, 565–571.
- (21) Kitamoto, D. A. I.; Isoda, H.; Nakahara, T. Functions and Potential Applications of Glycolipid Biosurfactants from Energy-Saving Materials to Gene Delivery Carriers. *J. Biosci. Bioeng.* **2002**, *94*, 187–201.
- (22) Singh, P.; Cameotra, S. S. Enhancement of Metal Bioremediation by Use of Microbial Surfactants. *Biochem. Biophys. Res. Commun.* **2004**, *319*, 291–297.
- (23) Herman, D. C.; Artiola, J. F.; Miller, R. M. Removal of Cadmium, Lead, and Zinc from Soil by a Rhamnolipid Biosurfactant. *Environ. Sci. Technol.* **1995**, *29*, 2280–2285.
- (24) Juwarkar, A. A.; Nair, A.; Dubey, K. V.; Singh, S. K.; Devotta, S. Biosurfactant Technology for Remediation of Cadmium and Llead Contaminated Soils. *Chemosphere* **2007**, *68*, 1996–2002.
- (25) Sandrin, T. R.; Chech, A. M.; Maier, R. M. A Rhamnolipid Biosurfactant Reduces Cadmium Toxicity during Naphthalene Biodegradation. *Appl. Environ. Microbiol.* **2000**, *66*, 4585–4588.
- (26) Slizovskiy, I. B.; Kelsey, J. W.; Hatzinger, P. B. Surfactant-Facilitated Remediation of Metal-Contaminated Soils: Efficacy and Toxicological Consequences to Earthworms. *Environ. Toxicol. Chem.* **2011**, *30*, 112–123.
- (27) Tan, H.; Champion, J. T.; Artiola, J. F.; Brusseau, M. L.; Miller, R. M. Complexation of Cadmium by a Rhamnolipid Biosurfactant. *Environ. Sci. Technol.* **1994**, 28, 2402–6.
- (28) Torrens, J. L.; Herman, D. C.; Miller-Maier, R. M. Biosurfactant (Rhamnolipid) Sorption and the Impact on Rhamnolipid-Facilitated Removal of Cadmium from Various Solids under Saturated Flow Conditions. *Environ. Sci. Technol.* **1998**, 32, 776–776.
- (29) Jain, D. K.; Lee, H.; Trevors, J. T. Effect of Addition of *Pseudomonas aeruginosa* UG2 Inocula or Biosurfactants on Biodegradation of Selected Hydrocarbons in Soil. *J. Ind. Microbiol.* **1992**, *10*, 87–93.
- (30) Providenti, M.; Flemming, C.; Lee, H.; Trevors, J. Effect of Addition of Rhamnolipid Biosurfactants or Rhamnolipid-Producing *Pseudomonas aeruginosa* on Phenanthrene Mineralization in Soil Slurries. *FEMS Microbiol. Ecol.* **1995**, *17*, 15–26.
- (31) Zhang, Y.; Miller, R. M. Enhanced Octadecane Dispersion and Biodegradation by a *Pseudomonas* Rhamnolipid Surfactant (Biosurfactant). *Appl. Environ. Microbiol.* **1992**, *58*, 3276–3282.
- (32) Zhang, Y.; Miller, R. M. Effect of a *Pseudomonas* Rhamnolipid Biosurfactant on Cell Hydrophobicity and Biodegradation of Octadecane. *Appl. Environ. Microbiol.* **1994**, *60*, 2101–2106.
- (33) Abbasi, Ĥ.; Aranda, F. J.; Noghabi, K. A.; Ortiz, A. A Bacterial Monorhamnolipid Alters the Biophysical Properties of Phosphatidy-

- lethanolamine Model Membranes. Biochim. Biophys. Acta, Biomembr. 2013, 1828, 2083–2090.
- (34) Bengtsson, T.; Holefors, A.; Liljeroth, E.; Hultberg, M.; Andreasson, E. Biosurfactants Have the Potential to Induce Defence Against Phytophthora infestans in Potato. *Potato Res.* **2015**, *58*, 83–90.
- (35) Miao, S.; Dashtbozorg, S. S.; Callow, N. V.; Ju, L.-K. Rhamnolipids as Platform Molecules for Production of Potential Anti-zoospore Agrochemicals. *J. Agric. Food Chem.* **2015**, *63*, 3367–3376
- (36) Stanghellini, M. E.; Miller, R. M. Biosurfactants: Their Identity and Potential Efficacy in the Biological Control of Zoosporic Plant Pathogens. *Plant Dis.* **1997**, *81*, 4–12.
- (37) Coss, C.; Carrocci, T.; Maier, R. M.; Pemberton, J. E.; Polt, R. Minimally Competent Lewis Acid Catalysts: Indium(III) and Bismuth(III) Salts Produce Rhamnosides (=6-deoxymannosides) in High Yield and Purity. *Helv. Chim. Acta* **2012**, *95*, 2652–2659.
- (38) Compton, A. A.; Deodhar, B. S.; Fathi, A.; Pemberton, J. E. Optimization of a Chemical Synthesis for Single-Chain Rhamnolipids. *ACS Sustainable Chem. Eng.* **2020**, *8*, 8918–8927.
- (39) Lefever, M. R.; Szabò, L. Z.; Anglin, B.; Ferracane, M.; Hogan, J.; Cooney, L.; Polt, R. Glycosylation of α -Amino Acids by Sugar Acetate Donors with InBr3. Minimally Competent Lewis Acids. *Carbohydr. Res.* **2012**, *351*, 121–125.
- (40) Zemplén, G.; Gerecs, A.; Hadácsy, I. Über die Verseifung acetylierter Kohlenhydrate. *Ber. Dtsch. Chem. Ges. B* **1936**, *69*, 1827–1829.
- (41) Neises, B.; Steglich, W. Simple Method for the Esterification of Carboxylic Acids. Angew. Chem., Int. Ed. Engl. 1978, 17, 522–524.
- (42) Oikawa, Y.; Sugano, K.; Yonemitsu, O. Meldrum's Acid in Organic Synthesis. 2. A General and Versatile Synthesis of Beta-Keto Esters. *J. Org. Chem.* **1978**, 43, 2087–2088.
- (43) Hill, K.; Rybinski, W. V.; Stoll, G. Alkyl Polyglycosides; Wiley: Weinheim, Germany, 1996.
- (44) Pantelic, I. Alkyl Polyglucosides: From Natural-Origin Surfactants to Prospective Delivery Systems; Woodhead Publishing: Cambridge, U.K., 2014.
- (45) Holmberg, K. Natural Surfactants. Curr. Opin. Colloid Interface Sci. 2001, 6, 148–159.
- (46) Hogan, D. E.; Tian, F.; Malm, S. W.; Olivares, C.; Palos Pacheco, R.; Simonich, M. T.; Hunjan, A. S.; Tanguay, R. L.; Klimecki, W. T.; Polt, R. R. M.; et al. Biodegradability and Toxicity of Monorhamnolipid Biosurfactant Diastereomers. *J. Hazard. Mater.* **2019**, *364*, 600–607.
- (47) Hogan, D. E.; Tian, F.; Malm, S. W.; Kegel, L. L.; Szabo, L.; Hunjan, A. S.; Klimecki, W. T.; Polt, R.; Pemberton, J. E.; Maier, R. M. Biodegradability and Toxicity of Cellobiosides and Melibiosides. *J. Surfactants Deterg.* **2020**, *23*, 715–724.
- (48) Aniansson, G. E. A. Dynamics and structure of micelles and other amphiphile structures. *J. Phys. Chem.* **1978**, 82, 2805–2808.
- (49) Eismin, R. J.; Munusamy, E.; Kegel, L. L.; Hogan, D. E.; Maier, R. M.; Schwartz, S. D.; Pemberton, J. E. Evolution of Aggregate Structure in Solutions of Anionic Monorhamnolipids: Experimental and Computational Results. *Langmuir* **2017**, *33*, 7412–7424.
- (50) Israelachvili, J. N.; Mitchell, D. J.; Ninham, B. W. Theory of self-assembly of hydrocarbon amphiphiles into micelles and bilayers. *J. Chem. Soc., Faraday Trans.* 2 **1976**, 72, 1525–1525.
- (51) Tanford, C. The Hydrophobic Effect: Formation of Micelles and Biological Membranes; Wiley: New York, 1973; pp 200–200.
- (52) Israelachvili, J. N. Intermolecular and Surface Forces; Acdemic Press: Amsterdam, 2011.
- (53) Israelachvili, J. N.; Ninham, B. W. Intermolecular Forces—The Long and Short of It. *J. Colloid Interface Sci.* 1977, 58, 14–25.
- (54) Knothe, G.; Dunn, R. O.; Bagby, M. O. Surface tension studies on novel allylic mono-and dihydroxy fatty compounds. A method to distinguisherythro/threo diastereomers. *J. Am. Oil Chem. Soc.* **1995**, 72, 43–47.
- (55) Ohta, A.; Hata, Y.; Mizuno, Y.; Asakawa, T.; Miyagishi, S. Phase Diagrams of Mixtures of Diastereomeric Salts of N -Acyl Amino Acid-

- Type Surfactants and Separation of Enantiomers. J. Phys. Chem. B 2004, 108, 12204–12209.
- (56) Jaeger, D. A.; Brown, E. L. G. Double-Chain Surfactants with Two Carboxylate Head Groups That Form Vesicles. *Langmuir* **1996**, 12, 1976–1980.
- (57) Rubingh, D. N. Mixed Micelle Solutions; Springer New York: Boston, MA, 1979; pp 337–354.
- (58) Rosen, M. J.; Hua, X. Y. Surface concentrations and molecular interactions in binary mixtures of surfactants. *J. Colloid Interface Sci.* **1982**, *86*, 164–172.
- (59) Rosen, M. J.; Hua, X. Y. Synergism in Binary Mixtures of Surfactants: II. Some Experimental Data. *J. Am. Oil Chem. Soc.* **1982**, 59, 582–585.
- (60) Hua, X. Y.; Rosen, M. J. Synergism in binary mixtures of surfactants. J. Colloid Interface Sci. 1982, 90, 212-219.
- (61) Scamehorn, J. F. An Overview of Phenomena Involving Surfactant Mixtures. In *Phenomena in Mixed Surfactant Systems*; ACS Symposium Series 311; American Chemical Society: Washington, DC, 1986; pp 1–27.
- (62) Shinoda, K. The Critical Micelle Concentration of Soap Mixtures (Two-Component Mixture). *J. Phys. Chem.* **1954**, *58*, 541–544.
- (63) du Nouy, P. L. An Interfacial Tensiometer for Universal Use. *J. Gen. Physiol.* **1925**, *7*, 625–631.
- (64) Zero, K.; Pecora, R. Dynamic Depolarized Light Scattering. In Dynamic Light Scattering; Springer US: Boston, MA, 1985; pp 59–83.
- (65) Pecora, R. In *Dynamic Light Scattering*; Pecora, R., Ed. Plenum Press: New York, 1985; p 420.
- (66) Piñeiro, L.; Novo, M.; Al-Soufi, W. Fluorescence Emission of Pyrene in Surfactant Solutions. *Adv. Colloid Interface Sci.* **2015**, 215, 1–12.
- (67) Mattay, J. Photochemistry of arenes Reloaded. *Angew. Chem., Int. Ed.* **2007**, 46, 663–665.
- (68) Butler, I. Removal of dissolved oxygen from water: A comparison of four common techniques. *Talanta* 1994, 41, 211–215.
- (69) Patrick, W. A.; Wagner, H. B. Method for Complete Deoxygenation of Water. *Anal. Chem.* **1949**, *21*, 752–753.
- (70) Grewer, C.; Brauer, H.-D. Mechanism of the Triplet-State Quenching by Molecular Oxygen in Solution. *J. Phys. Chem.* **1994**, 98, 4230–4235.
- (71) Hautala, R. R.; Schore, N. E.; Turro, N. J. A Novel Fluorescent Probe. Use of Time-Correlated Fluorescence to Explore the Properties of Micelle-Forming Detergent. *J. Am. Chem. Soc.* **1973**, 95, 5508–5514.
- (72) Gehlen, M. H.; De Schryver, F. C. Time-resolved fluorescence quenching in micellar assemblies. *Chem. Rev.* **1993**, 93, 199–221.
- (73) O'Connor, D. V.; Phillips, D. Time-Correlated Single Photon Counting; Academic Press: London, U.K., 1984; pp 288–288.
- (74) Tachiya, M. Application of a generating function to reaction kinetics in micelles. Kinetics of quenching of luminescent probes in micelles. *Chem. Phys. Lett.* **1975**, 33, 289–292.
- (75) Infelta, P. P.; Gratzel, M.; Thomas, J. K. Luminescence decay of hydrophobic molecules solubilized in aqueous micellar systems. Kinetic model. *J. Phys. Chem.* **1974**, *78*, 190–195.
- (76) Durbin, J.; Watson, G. S. Testing for Serial Correlation in Least Squares Regression. I. *Biometrika* **1950**, *37*, 409–428.
- (77) Durbin, J.; Watson, G. S. Testing for Serial Correlation in Least Squares Regression. II. *Biometrika* **1951**, 38, 159–178.
- (78) Warr, G. G.; Grieser, F.; Evans, D. F. Determination of Micelle Size and Polydispersity by Fluorescence Quenching. Experimental Results. *J. Chem. Soc., Faraday Trans.* 1 1986, 82, 1829–1838.
- (79) Miller, D. D.; Evans, D. F. Fluorescence Quenching in Double-Chained Surfactants. 1. Theory of Quenching in Micelles and Vesicles. *J. Phys. Chem.* **1989**, *93*, 323–333.
- (80) Munusamy, E.; Luft, C. M.; Pemberton, J. E.; Schwartz, S. D. Unraveling the Differential Aggregation of Anionic and Nonionic Monorhamnolipids at Air-Water and Oil-Water Interfaces: A Classical Molecular Dynamics Simulation Study. *J. Phys. Chem. B* **2018**, *122*, 6403–6416.

- (81) Gruen, D. W. R. A model for the chains in amphiphilic aggregates. 1. Comparison with a molecular dynamics simulation of a bilayer. *J. Phys. Chem.* **1985**, 89, 146–153.
- (82) Israelachvili, J. N.; Mitchell, D. J.; Ninham, B. W. Theory of Self-Assembly of Lipid Bilayers and Vesicles. *Biochim. Biophys. Acta, Biomembr.* 1977, 470, 185–201.
- (83) Munusamy, E.; Luft, C. M.; Pemberton, J. E.; Schwartz, S. D. Structural Properties of Nonionic Monorhamnolipid Aggregates in Water Studied by Classical Molecular Dynamics Simulations. *J. Phys. Chem. B* **2017**, *121*, 5781–5793.
- (84) von Szyszkowski, B. Experimental Studies on Capillary Properties of Aqueous Solutions of Fatty Acids. *Z. Phys. Chem.* **1908**, *64*, 385–414.
- (85) Ross, S.; Morrison, I. D. On the alleged ideality of szyszkowskilangmuir adsorption. J. Colloid Interface Sci. 1983, 91, 244–247.
- (86) Hill, T. L. Thermodynamics of Small Systems; W. A. Benjamin: New York, 1963.
- (87) Tanford, C. Interfacial Free Energy and the Hydrophobic Effect. *Proc. Natl. Acad. Sci. U. S. A.* 1979, 76, 4175–4176.
- (88) Warr, G. G.; Grieser, F. Determination of Micelle Size and Polydispersity by Fluorescence Quenching. *J. Chem. Soc., Faraday Trans. 1* **1986**, 82, 1813–1828.
- (89) Almgren, M.; Grieser, F.; Thomas, J. K. Dynamic and static aspects of solubilization of neutral arenes in ionic micellar solutions. *J. Am. Chem. Soc.* **1979**, *101*, 279–291.
- (90) Malliaris, A. Fluorescence probing in aqueous micellar systems: an overview. *Int. Rev. Phys. Chem.* **1988**, *7*, 95–121.
- (91) Marquardt, D. W. An Algorithm for Least-Squares Estimation of Nonlinear Parameters. J. Soc. Ind. Appl. Math. 1963, 11, 431–441.
- (92) Söderman, O.; Herrington, K. L.; Kaler, E. W.; Miller, D. D. Transition from Micelles to Vesicles in Aqueous Mixtures of Anionic and Cationic Surfactants. *Langmuir* 1997, 13, 5531–5538.
- (93) Miller, D. D.; Magid, L. J.; Evans, D. F. Fluorescence quenching in double-chained surfactants. 2. Experimental results. *J. Phys. Chem.* **1990**, *94*, 5921–5930.
- (94) Almgren, M. Diffusion-influenced deactivation processes in the study of surfactant aggregates. *Adv. Colloid Interface Sci.* **1992**, 41, 9–
- (95) Galla, H.-J.; Sackmann, E. Lateral diffusion in the hydrophobic region of membranes: use of pyrene excimers as optical probes. *Biochim. Biophys. Acta, Biomembr.* **1974**, 339, 103–115.
- (96) Thomas, J. K. The Chemistry of Excitation at Interfaces; American Chemical Society: Washignton, DC, 1984.
- (97) Collins, F. C.; Kimball, G. E. Diffusion-controlled reaction rates. *J. Colloid Sci.* **1949**, *4*, 425–437.
- (98) Choi, H. T.; Lipsky, S. Effect of perfluorocarbons on the ultraviolet absorption and fluorescence characteristics of some saturated hydrocarbon liquids. *J. Phys. Chem.* **1981**, *85*, 4089–4099.
- (99) Almgren, M.; Löfroth, J. E. Effects of polydispersity on fluorescence quenching in micelles. *J. Chem. Phys.* **1982**, *76*, 2734–2743.
- (100) Kegel, L. L.; Szabó, L. Z.; Polt, R.; Pemberton, J. E. Alkyl melibioside and alkyl cellobioside surfactants: effect of sugar headgroup and alkyl chain length on performance. *Green Chem.* **2016**, *18*, 4446–4460.
- (101) Nakajima, A. Fluorescence Lifetime of Pyrene in Different Solvents. *Bull. Chem. Soc. Jpn.* **1973**, *46*, 2602–2604.
- (102) Kalyanasundaram, K.; Thomas, J. K. Environmental effects on vibronic band intensities in pyrene monomer fluorescence and their application in studies of micellar systems. *J. Am. Chem. Soc.* **1977**, *99*, 2039–2044.
- (103) Meyer, E. A.; Castellano, R. K.; Diederich, F. Interactions with Aromatic Rings in Chemical and Biological Recognition. *Angew. Chem., Int. Ed.* **2003**, *42*, 1210–1250.
- (104) Takahashi, O.; Kohno, Y.; Nishio, M. Relevance of Weak Hydrogen Bonds in the Conformation of Organic Compounds and Bioconjugates: Evidence from Recent Experimental Data and High-Level ab Initio MO Calculations. *Chem. Rev.* **2010**, *110*, 6049–6076.

- (105) Bautista-Ibáñez, L.; Ramírez-Gualito, K.; Quiroz-García, B.; Rojas-Aguilar, A.; Cuevas, G. Calorimetric Measurement of the CH/π Interaction Involved in the Molecular Recognition of Saccharides by Aromatic Compounds. *J. Org. Chem.* **2008**, *73*, 849–857.
- (106) Terraneo, G.; Potenza, D.; Canales, A.; Jiménez-Barbero, J.; Baldridge, K. K.; Bernardi, A. A Simple Model System for the Study of Carbohydrate-Aromatic Interactions. *J. Am. Chem. Soc.* **2007**, *129*, 2890–2900.
- (107) Laughrey, Z. R.; Kiehna, S. E.; Riemen, A. J.; Waters, M. L. Carbohydrate-π Interactions: What Are They Worth? *J. Am. Chem. Soc.* **2008**, *130*, 14625–14633.
- (108) Morales, J. C.; Reina, J. J.; Díaz, I.; Aviñó, A.; Nieto, P. M.; Eritja, R. Experimental Measurement of Carbohydrate-Aromatic Stacking in Water by Using a Dangling-Ended DNA Model System. *Chem. Eur. J.* **2008**, *14*, 7828–7835.
- (109) Asensio, J. L.; Ardá, A.; Cañada, F. J.; Jiménez-Barbero, J. Carbohydrate-Aromatic Interactions. *Acc. Chem. Res.* **2013**, *46*, 946–954
- (110) Luft, C. M.; Munusamy, E.; Pemberton, J.; Schwartz, S. D. Molecular Dynamics Simulation of the Oil Sequestration Properties of a Nonionic Rhamnolipid. *J. Phys. Chem. B* **2018**, *122*, 3944–3952.